BBA - Biomembranes 1862 (2020) 183420

Contents lists available at ScienceDirect

BBA - Biomembranes

journal homepage: www.elsevier.com/locate/bbamem

Complexity of seemingly simple lipid nanodiscs

Piotr Stepien[a,b], Bozena Augustyn[a,c], Chetan Poojari[d,e], Wojciech Galan[f], Agnieszka Polit[g], Ilpo Vattulainen[d,h,i], Anna Wisnieska-Becker[a,*], Tomasz Rog[d,*]

[a] Department of Biophysics, Jagiellonian University, Krakow, Poland
[b] Bionanoscience and Biochemistry Laboratory, Malopolska Centre of Biotechnology, Jagiellonian University, Krakow, Poland
[c] Ardigen, Podole 76, 30-394 Krakow, Poland
[d] Department of Physics, University of Helsinki, Helsinki, Finland
[e] Theoretical Physics and Center for Biophysics, Saarland University, 66123 Saarbrücken, Germany
[f] Department of Computational Biophysics and Bioinformatics, Jagiellonian University, Krakow, Poland
[g] Department of Physical Biochemistry, Jagiellonian University, Krakow, Poland
[h] Computational Physics Laboratory, Tampere University, Tampere, Finland
[i] MEMPHYS – Center for Biomembrane Physics, Denmark

ARTICLE INFO

Keywords:
Electron paramagnetic resonance
Molecular dynamics simulations
Lipids ordering
Membrane proteins

ABSTRACT

Lipid nanodiscs are macromolecular assemblies, where a scaffold protein is wrapped around a nanosized disc of a lipid bilayer, thus protecting the hydrocarbon chains at the disc edges from unfavorable interactions with water. These nanostructures have numerous applications in, e.g., nanotechnology and pharmaceutics, and in investigations of membrane proteins. Here, we present results based on atomistic molecular dynamics simulations combined with electron paramagnetic spectroscopy measurements on the structure and dynamics of lipids in single-component nanodiscs. Our data highlight the existence of three distinctly different lipid fractions: central lipids residing in the center of a nanodisc, boundary lipids in direct contact with a scaffold protein, and intermediate lipids between these two regions. The central lipids are highly ordered and characterized by slow diffusion. In this part of the nanodisc, the membrane is the thickest and characterized by a gel-like or liquid-ordered phase, having features common to cholesterol-rich membranes. The boundary lipids in direct contact with the scaffold protein turned out to be less ordered and characterized by faster diffusion, and they remained in the liquid-disordered phase even at temperatures that were somewhat below the main phase transition temperature (Tm). The enthalpies associated with the central-boundary and central-intermediate transitions were similar to those observed for lipids going through the main phase transition. Overall, the study reveals lipid nanodiscs to be characterized by a complex internal structure, which is expected to influence membrane proteins placed in nanodiscs.

1. Introduction

Lipid nanodiscs are macromolecular assemblies comprised of a patch of a lipid bilayer surrounded by membrane scaffold proteins (MSPs) shielding the lipid hydrocarbon acyl chains from contact with water molecules [1]. These nano-devices have been developed for various applications including, e.g., drug delivery [2,3], fabrication of nanosensors [4], and catalytic devices [5]. Yet, their main application areas are structural and functional studies of membrane proteins [6,7].

Membrane proteins are key players in various cellular processes such as signaling, cell adhesion, and energy conversion [8]. They are coded by 20–30% of genes in the majority of known genomes [9,10]. Membrane proteins also constitute two thirds of proteins targeted by drugs, and they bind approximately 50% of small molecular therapeutic substances [11–13]. Nonetheless, since membrane proteins are insoluble in polar solvents, they are difficult to explore and thus underrepresented with regard to structural and functional studies of biomolecular systems.

What is needed to investigate the function of membrane proteins? One obviously needs the proteins, and functional circumstances aimed at stabilizing their structure and fostering their activity.

Production of membrane proteins for in vitro experiments is usually not a problem. A trickier task is protein stabilization that should be possible regardless of whether proteins are expressed in bacterial cells, eukaryotic cells, or under cell-free conditions. There are several ways to accomplish this, such as, one can use detergents or other hydrophobic

* Corresponding authors.
E-mail addresses: anna.m.wisniewska@uj.edu.pl (A. Wisnieska-Becker), tomasz.rog@helsinki.fi (T. Rog).

https://doi.org/10.1016/j.bbamem.2020.183420
Received 11 February 2020; Received in revised form 26 June 2020; Accepted 7 July 2020
Available online 23 July 2020

agents that form micellar structures around the hydrophobic domains of proteins [14]. However, the stability alone does not guarantee that the given proteins would function correctly. To do so, the environment around membrane proteins should be close to native conditions. This requirement has created pressure to develop new methods that would ensure that the environment used to explore protein behavior is as close as possible to realistic conditions. Examples of methods that have been found to largely satisfy this condition include reconstitution of membrane proteins in liposomes, use of supported bilayers, and utilization of cubic phases [15,16].

The approach that has been suggested most recently is based on nanodiscs as carriers of membrane proteins [7,17]. Together with cryo-electron microscopy, they have been employed to determine numerous new structures of membrane proteins [6,18,19]. Perhaps the most impressive example in this context is the reconstitution of the full-length active-state insulin receptor [20].

Due to their exceptional potential in nanoscience, nanodiscs have been a subject of intense studies, with an objective to optimize their properties for selected applications [1,17,21]. For instance, to strengthen the stability of nanodiscs, their properties have been optimized by adjusting their lipid composition [22], or by modifying the scaffold proteins [23]. The size of nanodiscs can also be optimized by varying the length of MSPs [24,25], which provides a means to accommodate proteins of various sizes, as well as larger protein oligomers [7]. Since the lipid composition of nanodiscs can be precisely controlled, one can also explore membrane proteins allosterically bound to specific lipids [26–28].

The presence of MSPs in nanodiscs is crucial, since they stabilize the structure of nanodiscs. However, there is evidence suggesting that MSPs also alter the conformation of lipids' hydrocarbon chains and polar headgroups, as well as lipid dynamics [29]. Previous studies on nanodiscs have suggested that the structures of lipids in nanodiscs are different from those in planar lipid bilayer systems [30]. Meanwhile, membrane proteins such as mechanosensitive channels are sensitive to the pressure profile exerted on the protein [31], and allosteric binding of lipids to membrane protein structures can be sensitive to the conformations of the lipids [27]. Given these factors, understanding the internal structure and dynamics of lipid nanodiscs is exceptionally important.

In this work, we used all-atom molecular dynamics (MD) simulations (Fig. 1A) and electron paramagnetic resonance (EPR) measurements to investigate the structure of nanodiscs and the dynamics of their lipids. The nanodiscs explored here are lipid membranes (composed of either monounsaturated 1-palmitoyl-2-oleoyl-sn-glycero-3-phosphocholine (POPC) or saturated 1,2-dimyristoyl-sn-glycero-3-phosphocholine (DMPC)) surrounded by an MSP, whose length largely determines the size of the nanodisc. For this purpose, we used MSP1D1 and MSP1E3D1 proteins, which generated nanodiscs of approximately 9.7 nm and 12.8 nm in size, respectively.

The results highlight that lipids in nanodiscs can be decomposed into three distinctly different fractions: central lipids residing in the center of a nanodisc, boundary lipids in direct contact with a scaffold protein, and intermediate lipids between these two regions. The lipid properties in these three cases are clearly different and demonstrate that lipid nanodiscs are characterized by a complex internal structure.

2. Materials and methods

2.1. Materials for nanodiscs and liposomes

POPC and DMPC lipids were purchased from NOF Europe and the PC spin labels from Avanti Polar Lipids. The Plasmids for MSPs expression were purchased from Addgene [7,32]. All other necessary compounds for protein purification and buffer preparation were purchased from Sigma Aldrich Europe.

2.2. Sample preparation

The experimental setup consisted of measurements of MSP1D1 and MSP1E3D1 nanodiscs and multilamellar liposomes prepared using either POPC or DMPC lipids. A set of paramagnetic probes, i.e., T-PC, 5-PC, 10-PC, 12-PC, and 16-PC was utilized. T-PC has its paramagnetic TEMPO moiety attached to the headgroup of PC, and the n-PC labels have a DOXYL moiety attached to the n^{th} carbon atom along the acyl chain of PC (Fig. 1B). In this way, the information about the motion of specific parts of a lipid molecule can be acquired as the paramagnetic centers provide information about the structure of a bilayer at a specific depth. For each of the studied systems, samples containing all of the described PC labels were prepared using 1% of the total lipid concentration for n-PC labels and 2% for the T-PC label. This concentration avoids labels interacting with each other as well as altering the structure of the studied membranes. Both the liposome and nanodisc samples for the EPR measurements were prepared and checked for quality as described in previous work [33].

2.3. EPR measurements

The EPR measurements were conducted using the Bruker EMX spectrometer equipped with EMX ER 4141 VT temperature control unit. Samples were placed in a gas-permeable methylpentene plastic, TPX (i.d. 0.6 mm) capillary, and deoxygenated inside the resonator using nitrogen fumes from the temperature control unit. All samples were

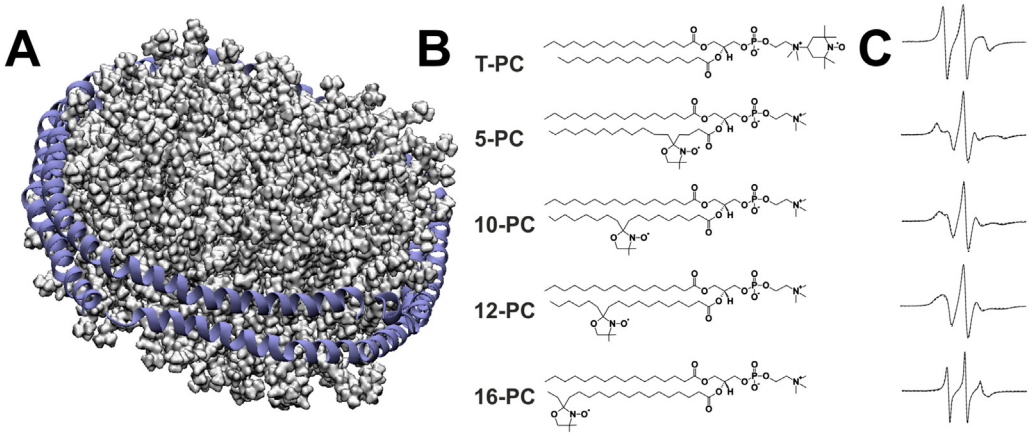

Fig. 1. (**A**) An all-atom model of MSP1D1/POPC nanodiscs. (**B**) PC-based labels used for probing various depths within a lipid bilayer. Abbreviations of lipids' names are described in the text. (**C**) Corresponding experimental spectra in MSP1D1/POPC nanodiscs measured at 293 K.

measured at both 293 and 310 K. Additionally, the samples containing a 12-PC label were measured within the temperature range, with 2 K increments. The range for POPC samples was from 275 to 293 K and for DMPC from 293 to 313 K. This special treatment for the 12-PC label is due to its sensitivity to protein bound lipids [34]. It was used here to provide information about MSP-bound lipids as described in the boundary lipids section. After the measurements in the described temperatures, the samples were rapidly frozen at 120 K to perform polarity measurements [35]. Freezing the samples was done as the last step of measurements to prevent any changes to the studied systems upon thawing.

2.4. Molecular dynamics simulations

The initial structures of nanodiscs and planar lipid bilayers were built using the CHARMM-GUI [36,37] server (Fig. 1A; Fig. S16). MSP1D1 and MSP1E3D1 nanodiscs were composed either of POPC or DMPC lipids that were distributed symmetrically on the two leaflets. As a control, POPC and DMPC planar lipid bilayers were also prepared. The structures were next solvated with water using the TIP3P water model [38] and neutralized by Na^+ counterions. Further, 100 mM of NaCl salt was added to match the experimental saline condition. The exact compositions of all the systems are given in Table S1. It is worth noting that the number of lipids in nanodiscs that are studied in experiments is not precisely known. Therefore, when simulation models for nanodiscs were being made, the number of lipids was estimated based on the surface area per lipid molecule. Here it is worth pointing out that the number of lipids in a nanodisc may affect some of their properties, e.g., the shape as shown in previous studies [39–41]. However, since the key objective in this work was to figure out whether there are different regions in nanodiscs with different properties, the quantitative simulation results are less important than the trends predicted by our simulations. Nonetheless, if there would be significant interest to resolve the shapes of nanodiscs (see Fig. S1), an alternative method would be to prepare nanodisc structures through self-assembly simulations. However, since the time scale of such atomistic simulations would be in the range of 10–100 μs, coarse-grained simulations would be a more appropriate approach to explore this topic [42].

Initially, the systems were subjected to energy minimization using 5000 steps of the steepest-descent algorithm. The optimized systems were equilibrated under NVT conditions using the Berendsen algorithm [43] to regulate the temperature (310*K*) with separate heat baths for the membrane, the protein, and solvent/ions. The time constant for temperature coupling was set to 1.0 ps. The pre-equilibration period was 75 ps for nanodiscs and 1 ns for bilayer systems. As a second step for equilibration, nanodiscs were simulated for 300 ps under NPT conditions with pressure (1 bar) controlled with the Berendsen method [43] using an isotropic scheme, whereas the bilayers were simulated for 1 ns with pressure (1 bar) controlled with the Parrinello–Rahman barostat [43] using the semi-isotropic pressure coupling scheme. During the equilibration steps, position restraints were applied to the lipid and protein atoms.

In the production runs, all applied restraints were removed. Here, the temperature was regulated using the Nose-Hoover thermostat [44,45], and the pressure was controlled using the Parrinello–Rahman barostat [46]. The time constants for pressure and temperature coupling were set to 5.0 and 1.0 ps, respectively. The isothermal compressibility was set to 4.5e-5 bar^{-1}. The electrostatic interactions were treated using the Particle-Mesh Ewald (PME) [47] method with a Coulomb cut-off distance of 1.2 nm. For the van der Waals interactions, we used a cut-off method with a Lennard-Jones cut-off distance of 1.2 nm. The neighbor search was performed using the Verlet cutoff-scheme, and the neighbor list was updated every 20 steps. The covalent bonds between hydrogen and heavy atoms were constrained using the Linear Constraint Solver (LINCS) algorithm [48]. The time step was set to 2 fs. The CHARMM36 force field [49] was used to describe protein and lipids, while for water we used the CHARMM version of the TIP3P model [38]. Simulations were carried out using the GROMACS 5 molecular dynamics simulation package [50]. The analysis was performed for the last 300 ns for the MSP1D1 nanodiscs and for the last 200 ns for the MSP1E3D1 nanodiscs and planar lipid bilayer systems. Analysis was performed using the VMD [51] program, GROMACS tools for analyzing membrane trajectories [52] and in-house codes.

3. Results and discussion

3.1. Structure across lipid bilayer in nanodiscs

Previous studies have established that the packing of lipids in nanodiscs is more prominent compared to liposomes. Nuclear magnetic resonance (NMR), EPR, and time-resolved fluorescence spectroscopy studies utilizing lipid-based probes have shown tighter packing of acyl chains in nanodiscs both above and below the main phase transition temperature (T_m) [29,30,33,53]. Additionally, small-angle neutron scattering (SANS) measurements have shown that the entropy in nanodiscs is higher compared to liposomes [30]. However, the conclusions of these studies were based on an average taken over all lipids in a nanodisc, therefore disregarding possible heterogeneity within a nanodisc. In the present work, we explore this matter in more detail by assessing the heterogeneity in the organization and motion of lipid acyl chains upon introduction of an MSP into a lipid nanodisc. To this end, we gauge nanodisc properties at different depths in a nanodisc using T-PC, 5-PC, 10-PC, 12-PC, and 16-PC labels, see Fig. 1B. Here the number stands for the carbon atom number along the acyl chain in which the label is attached, while in T-PC, the label is attached to the lipid headgroup. To complement these experimental investigations, we also performed atomistic MD simulations to unravel the same questions but in full atomic detail.

EPR measurements provide physical insight into nanodisc properties through three useful parameters:

- The S_0 order parameter, which provides information about structural aspects of the semi-cone in which the motion of the paramagnetic moiety takes place (Fig. S3, Eq. (S1)).
- The $R_\perp$ parameter, which describes the rate of motion (diffusion) of labelled molecules.
- The $2A_{zz}$ parameter, which reveals information about the polarity of the probe environment measured at 120 K (Fig. S2).

In atomistic MD simulations, we consider similar nanodisc properties using a number of very useful physical variables:

- The S_{CD} order parameter (Eq. (S9)) and the rotational autocorrelation function (RCF) (Eq. (S7)) that also provide information of the system's local structure and dynamics.
- The mean-squared displacement (MSD) of molecules' centers of mass (Eq. (S10)) used to explore the diffusion of lipids within a nanodisc.
- Density profiles of water and the polar groups of lipids to elucidate the polarity of the membrane environment.

We observe that the $R_\perp$ parameter is significantly smaller in nanodiscs for the 12-PC and 16-PC labels compared to liposomes (Fig. 2A, B), indicating lower mobility of lipid acyl chains within the inner portions of nanodiscs. This result is supported by MD simulations, which show lower mobility of lipids in nanodiscs in terms of rotational and translational diffusion (Fig. S19, S20, S21, and Table S4). Additionally, the anisotropy in the motion of labelled lipids is higher in nanodiscs as shown by angles probed by the 16-PC label, suggesting tighter packing in nanodiscs compared to liposomes (Fig. S11).

Increased order of the lipid bilayer in nanodiscs is visible from the S_0 profiles: both POPC and DMPC acyl chains display higher order, the

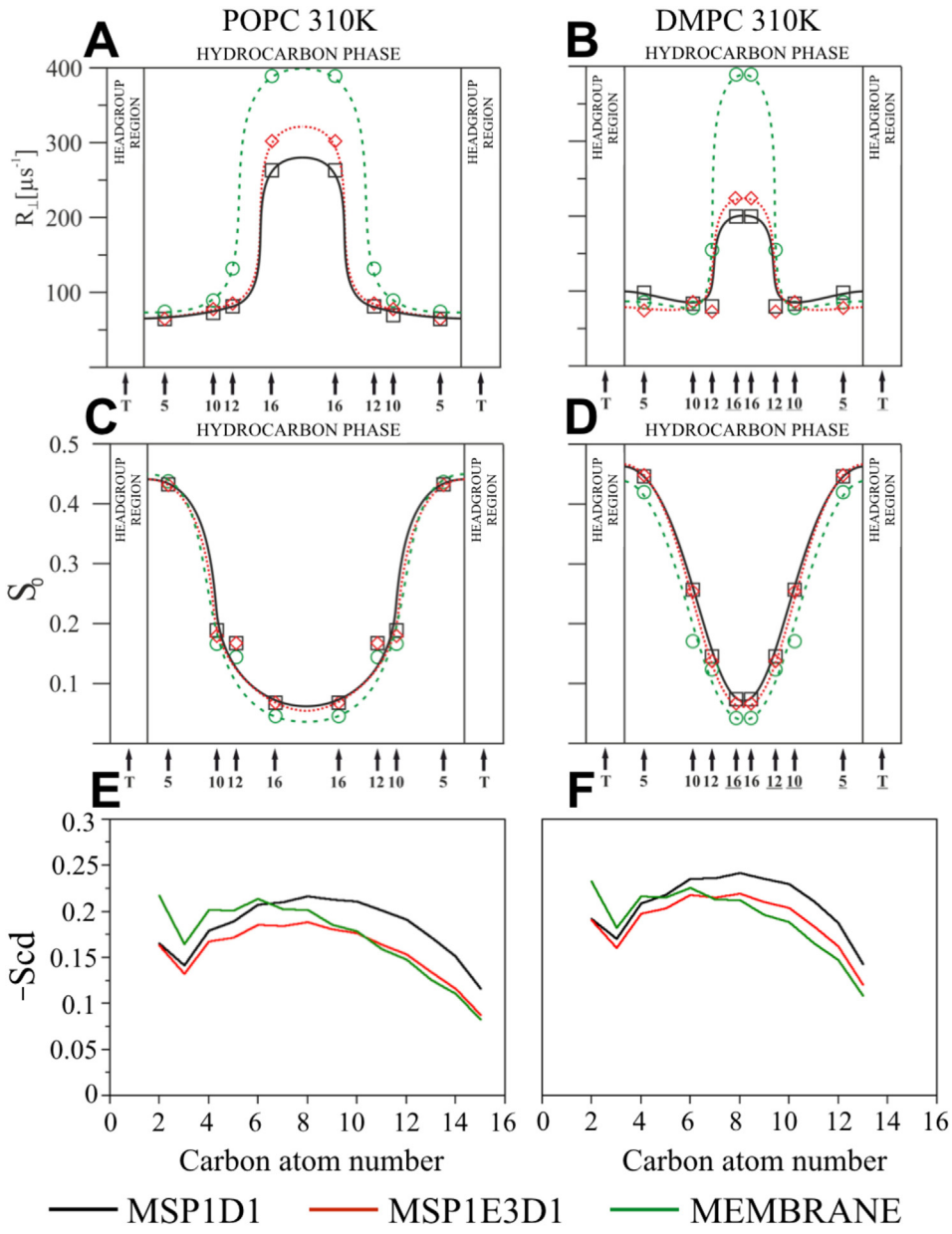

Fig. 2. Experimental data for parameters (A, B) $R_{\perp}$ and (C, D) S_0 measured at 310 K for POPC and DMPC, respectively. (E) Simulation results for the S_{CD} order parameter profile along the *sn*-1 chain of POPC. (F) Similar order parameter data for DMPC. Color code for the results given: green (membranes (liposomes or planar lipid bilayers)), red (MSP1E3D1), and black (MSP1D1). (For interpretation of the references to color in this figure legend, the reader is referred to the web version of this article.)

effect being more pronounced for DMPC nanodiscs (Fig. 2C, D). For POPC, the ordering effect is more clearly seen at lower temperatures (Fig. S12B). MD simulations showed an increase in the order of the lipid acyl chain segments located in the bilayer core, starting from the 5-7th segment and extending until the end of the chain, and decreased order for the first 4–6 segments (Fig. 2E, F). The difference in the ordering of acyl chains observed in planar lipid bilayers and nanodiscs as observed in MD simulations seems to be more significant than in experimental data. While direct comparison of the simulation and experimental results is not possible, one can argue that there are two likely reasons. First, due to a slight affinity of the labels towards the polar region of the bilayer [54], the labels sample a larger section of a bilayer in the direction of the bilayer normal than unlabeled segments. Second, the numbers of lipids used to construct the nanodiscs in the simulation models do not precisely match the experimental conditions. As illustrated in Fig. S1, the size of experimentally studied nanodiscs characterized by their hydrodynamic radius has a broad distribution.

The increase in the order of the acyl chains may be interpreted as an increase in the packing of lipid acyl chains. This is reflected in the profiles of parameter $2A_{zz}$ (polarity profiles). Polarity in the central region of the nanodiscs is much lower than in the liposomes (Fig. 3B, D), resulting from lower water penetration into nanodiscs due to tighter packing of the lipid acyl chains. Moreover, the lipid bilayer in nanodiscs is thicker when compared to the planar lipid bilayer, and this obviously results from a more packed configuration of the lipid acyl chains, which lengthens the chains and thickens the bilayer region. Interestingly, segments of the lipid acyl chains located close to the membrane surface show lower ordering/packing than in planar lipid bilayers (Fig. 2E, F). This result is in line with our previous study, which showed that the packing in the polar headgroup region of nanodiscs is lower than in liposomes [33]. It is therefore not surprising that we see an increase in polarity as observed by the increase of $2A_{zz}$ for T-PC (Fig. 3B, D).

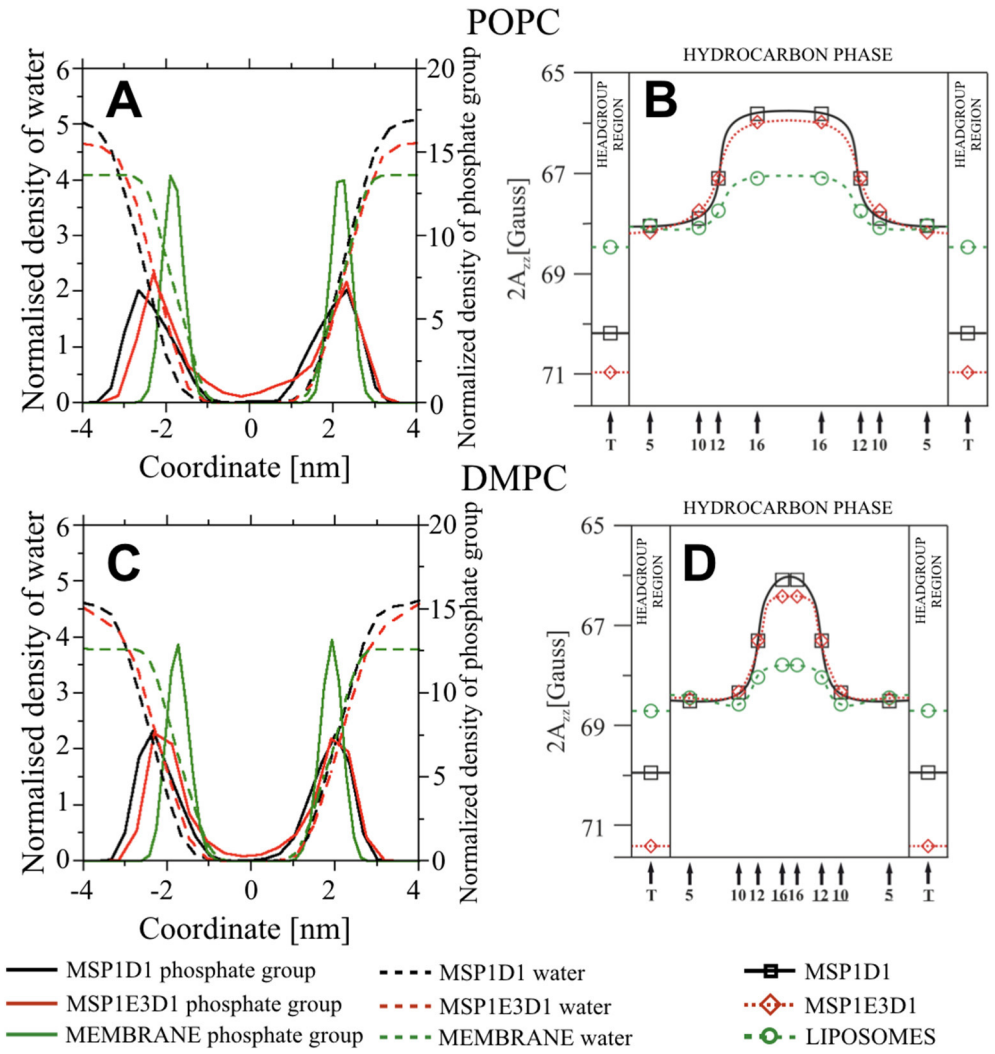

Fig. 3. (A, B) Density profiles obtained from MD simulations and (C, D) polarity profiles obtained from EPR measurements for POPC and DMPC nanodiscs (MSP1D1 and MSP1E3D1) and the full membrane. In panels (A) and (C) a scale for the density of water is shown at the left bar, and for the density of phosphate groups on the right bar. In panels (B) and (D), the spin label positions are shown by arrows in the *x*-axis, and the upward changes in the *y*-axis indicate decrease in polarity.

Increased polarity corresponds to increased hydration of headgroups observed in MD simulations (see the density profile of water, Fig. 3A, C) and a number of direct hydrogen bonds between water and lipids (Table S3).

Analysis of the T-PC label spectra in nanodiscs shows increased mobility, decreased value of S_0 (Fig. S14) and higher wobbling motion as characterized by the angular distribution sampled by this spin label (Fig. S15). This result is in agreement with the density plots of phosphate atoms, which indicate a thicker and more hydrated layer occupied by the headgroups (Fig. 3A, C). This effect is, however, in part related to lateral inhomogeneity of the bilayer region in nanodiscs (see below), demonstrated by differences in bilayer thickness in the central region of nanodiscs (planar surface) and next to the MSP (a slightly negatively curved surface). This indicates that the surface of the bilayer in nanodiscs is also inhomogeneous, allowing higher mobility and hydration of the headgroup in the vicinity of the MSP and lower mobility and hydration in the central section of the disc.

Interpretation of the RCF determined from MD simulations for the headgroups is particularly tricky, as three components are needed to obtain a satisfactory fit to the simulation data, while experimental data can be fitted with a single parameter. A closer look at the data (Table S4) shows an increase in A0 (Eq. (S8)) for nanodiscs, which is part of the amplitude not associated with the time constant but reflects the cone angle of rotation, therefore being related to the order parameter. At the same time, we observe an increase in the amplitude of two faster modes of motion and a decrease in the amplitude of the third slow component. These can be interpreted as increased mobility, which agrees with the experimental data. However, a simultaneously observed larger value for A0 indicates a larger order parameter, which disagrees with experiments. However, what should be considered is the structure of the labelled lipid, which effectively has a much larger headgroup. It is expected that it segregates into a region close to the MSP where the level of packing is lower in comparison to the center of the disc.

3.2. Lateral inhomogeneity of nanodiscs

A recent report showed that bilayers in nanodiscs contain lipids which are in a gel-like state even above the main phase transition, as well as lipids in the fluid state below the main phase transition temperature [53]. In our study, we also acquired data, which shows the presence of lipids in the fluid state in temperatures below their T_m. For DMPC nanodiscs at 293 K, the S_0 value for the 5-PC label (Fig. S13B) is significantly lower than the value observed in liposomes, which is typical for the gel phase. Further, the $R_\perp$ value for the 16-PC label is higher in nanodiscs than in liposomes (Fig. S13A). Both of these results suggest that there are fluid-state lipids below the main phase transition

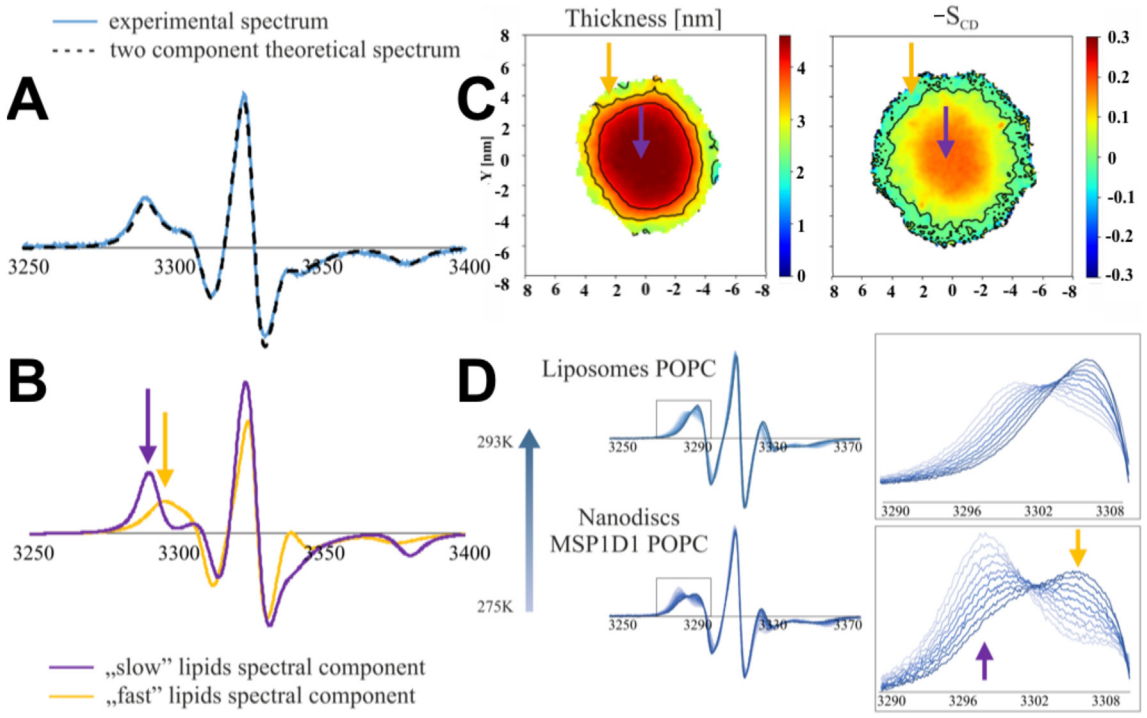

Fig. 4. (A) Exemplary two-component spectra (dashed line) fitted to experimental data of the 12-PC spectra (blue line) for POPC/MSP1D1 nanodiscs measured at 275 K. (B) Slow and fast spectral components of fitted components (violet and yellow lines, respectively). (C) 2D maps showing bilayer thickness (left panel) and lipid *sn*-1 and *sn*-2 acyl chain order parameter (right panel) for MSP1D1 nanodiscs at 310 K; the maps were calculated using a script from ref. [[52]]. (D) Temperature dependencies of the EPR spectra of 12-PC. Slow and fast populations are denoted with violet and yellow arrows, respectively, on the EPR spectra and 2D maps. (For interpretation of the references to color in this figure legend, the reader is referred to the web version of this article.)

of DMPC. Meanwhile, studies of lipid bilayers in nanodiscs using differential scanning calorimetry (DSC), small angle X-ray scattering (SAXS), and MD simulations [24,42,55–57] showed that there are two populations of lipids in nanodiscs — boundary lipids located in the proximity of an MSP and central (bulk) lipids located in the middle of the disc.

In order to study both populations of lipids in different phases, we employed 12-PC. For the 12-PC spin label, the paramagnetic moiety lies in the part of the membrane which is most sensitive to factors modifying membrane fluidity, thus allowing detection of lipids interacting with proteins [34]. Indeed, fitting the experimental spectra of 12-PC with one population of spin labels does not provide satisfactory fits, suggesting that two populations of spin labels with different S_0 and $R_\perp$ are required to provide fits of good quality (Fig. 4A, B). We used the data acquired from MD simulations to distinguish and assign the two populations of fast and slow lipids that could be expected to form separate regions in the nanodiscs. Spatial distribution of parameters such as bilayer thickness and S_{cd} (averaged along the bilayer normal) in the membrane plane (2D maps) show that the bilayer in the boundary region has a lower thickness, and the lipid acyl chains in this region are less ordered (Fig. 4C). Based on the 2D maps, we can estimate the maximum thickness of the central area in the nanodiscs. For MSP1D1 nanodiscs with POPC lipids, the thickness is around 4.5 nm, which is higher than the thickness observed in planar lipid bilayers (4.1 nm). These central lipids are highly ordered with extended acyl chains, thus their behavior matches the idea of slow lipids. Profiles of the S_{CD} parameters calculated for lipids located in the central cylinder and the three rings around it (Fig. 5) show a significant increase in the order in the central cylinder and very low order near the MPS. The level of ordering in the central cylinder is similar to the order of tails in the gel phase, although the shape of the profile differs; in the gel phase, the profile is flat with a value of S_{CD} around 0.31 [58]. The increase of the order in the tail region is comparable to the effect of cholesterol at a concentration of 25 mol% [22]; thus, it is similar to the Lo phase. The increase of the tail order is larger in MSP1D1, that is the nanodisc with a smaller diameter. A similar difference in the bilayer thickness between the central and boundary lipids in nanodiscs was previously reported based on both SAXS experiments and MD simulations [24,56].

To investigate the changes in the behavior of both central and boundary lipids upon a change in temperature, we collected EPR spectra for the POPC-based system in the temperature range of 275–293 K, and for the DMPC-based system in the range of 293–313 K. For nanodiscs, a discrete transition between the two populations of lipids is visible as opposed to liposomes for which only one population of lipids exist at all temperatures (Fig. 4D). This discrete transition is particularly well visible in the low-field component of EPR spectra. For temperatures well above the main phase transition (no thermal contribution on lipids changing their phase), nanodiscs' spectra have an isosbestic point indicating a two-state model (Fig. 6A). Knowing the relative amplitude of spectra for both populations, the proportions of the central and boundary lipids populations could be estimated. Nanodisc spectra with a clear isosbestic point show a linear trend in the van't Hoff plot (Fig. 6C). Based on the van't Hoff plot, the thermodynamic parameters characterizing the translocation of lipids from the central to the boundary regions were calculated (Table 1).

Additionally, the S_0 and $R_\perp$ parameters acquired from temperature scans for both fast and slow lipids (Fig. 6B) allowed us to describe the changes in bilayers upon an increase in temperature, along with phases in which lipids are present in both central and boundary regions at different temperatures. At all temperatures, the fast (boundary) lipids are in the liquid-disordered phase (Fig. 6). With increasing temperature, their packing (as reported by S_0) decreases and the rotational frequency $R_\perp$ steadily increases, which is typical for lipids in the liquid-disordered phase. In addition, the bilayer thickness of boundary lipids is similar to that observed in a planar lipid bilayer (Fig. 4B corresponds to nanodiscs and not to planar bilayer systems), which are in the liquid-disordered phase [59]. The liquid-disordered contribution in the NMR spectra measured below the main phase transition [53], is due to fast

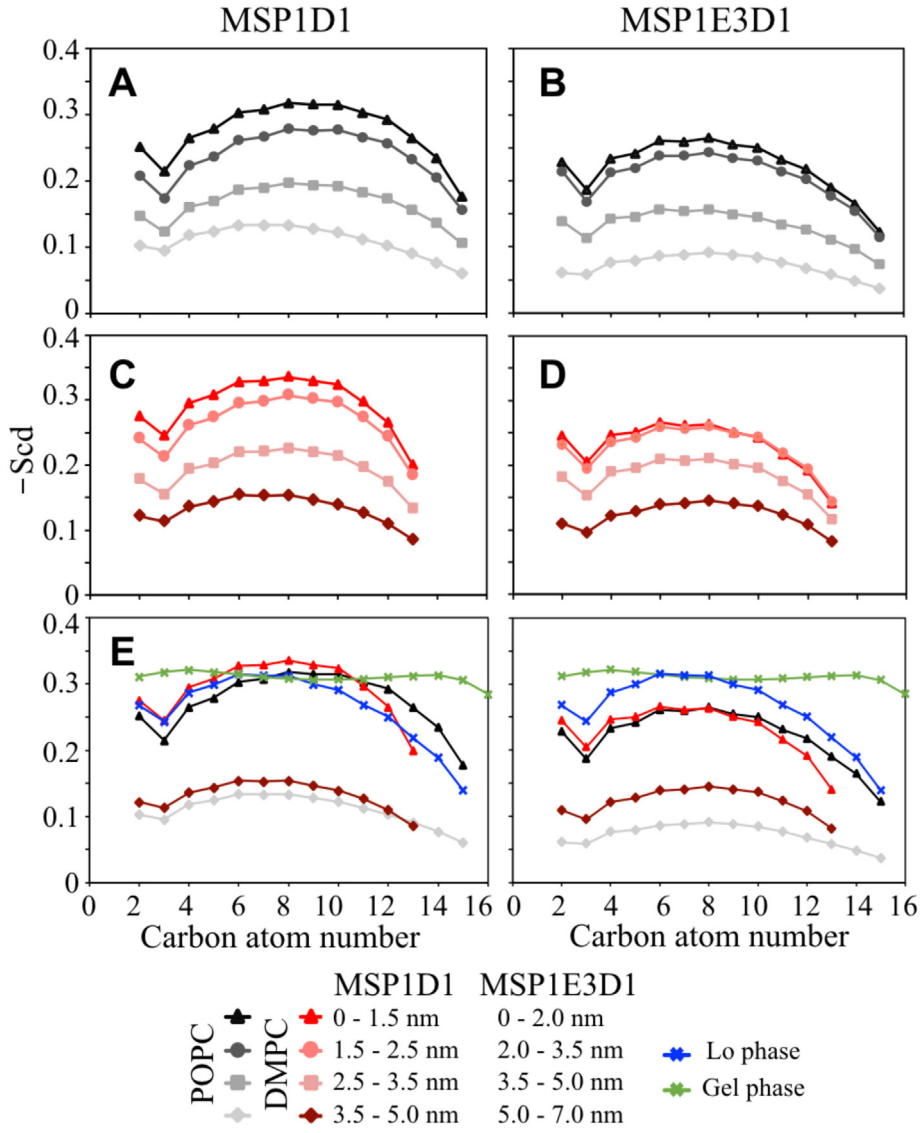

Fig. 5. Profiles of the order parameter S_{CD} along the *sn*-1 tail of POPC (A, B) and DMPC (C, D) for four compartments at different distances from the disc center. Panels E and F show S_{CD} profiles for the central cylinder and in direct neighborhood of the MPS in comparison with the profile obtained in prior studies for bilayers in the gel phase [58] and the Lo phase [22].

lipids, as is also the decrease in S_0 of the 5-PC label (Fig. S13B) observed in this study. This information is critical regarding membrane protein reconstitution since these lipids provide a non-gel environment for proteins in a broader range of temperatures than in liposomes. This is an advantage, since the activity of membrane proteins was shown to be reduced by gel-state lipids [60,61].

The slow (central) lipids behave differently at lower temperatures. Results of both S_0 and $R_\perp$ are within the range of values that are typical for the gel state. However, at higher temperatures (POPC at 310 K, DMPC around 303–313 K) when the S_0 parameter stays within the range that is typical for the ordered state (with extended acyl chains), $R_\perp$ increases quickly, and the measured spectra start resembling data that are typical for lipids in the liquid-ordered state (Fig. 7) [62,63]. This phase is typical for lipids in the presence of cholesterol, where the steric interactions with cholesterol molecules do not allow chains to adopt disordered structures and also prevent collective hexagonal packing, while the rotation of molecules is yet rapid [62,63]. The S_0 and $R_\perp$ values for the 12-PC label in the center of nanodiscs is similar to values reported for DMPC liposomes with 50% cholesterol [64]. In agreement with the experimental data, MD simulations showed that the lipid bilayer in the central region is thicker than in the respective planar lipid bilayers (Fig. S23) and a close examination of MD snapshots of central lipids confirmed this conclusion (Fig. S24).

Another interesting aspect of the lipid dynamics in nanodiscs is their translocation between the two populations. As shown by values calculated from the van't Hoff plot, the enthalpies of transition ($\Delta H^0_{Fast\rightarrow Slow}$) between the boundary and central lipids are similar to those observed for lipids going through the main phase transition (Table 1). Further, the number of lipids in the population of fast lipids increases with increasing temperature — this means that the amount of boundary lipids, affected by the presence of an MSP, also increases. This is consistent with a previous report [55], which showed that upon heating the radius of nanodiscs slightly increases, allowing more lipids to melt.

The number of lipids under the influence of an MSP was previously reported to be about 67% [55], which is in good agreement with 55.6–69.4% observed in the experiments of the present work (Table 1). Based on the order parameter and bilayer thickness 2D maps, it is possible to estimate the number of lipids influenced by the MSP, and the number of central lipids, whose properties do not change. These considerations give an estimate of 38–64% for the ratio of lipids influenced by the MSP, which is a bit lower than the experimental values.

Using distance criteria, the MD simulations provide an estimate for

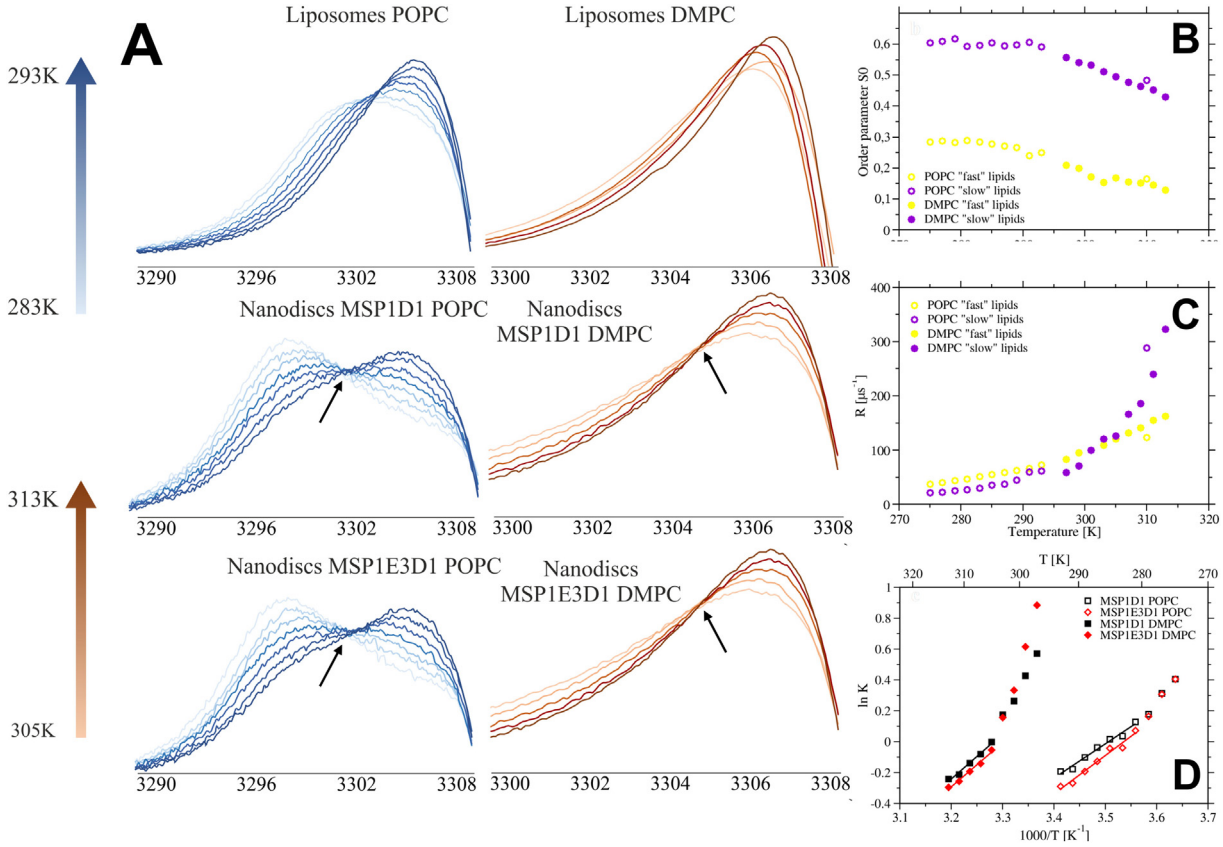

Fig. 6. (A) Low-field component 12-PC spectrum changes in the studied system as a function of temperature. Only spectra displaying the isosbestic point (black arrow) are shown here. Temperature dependencies of (B) S_0 and (C) $R_\perp$ for fast and slow lipid populations of 12-PC for POPC and DMPC MSP1D1 nanodiscs. The trend was similar for MSP1E3D1 nanodiscs (data not shown). (D) Van't Hoff plot for MSP1D1 and MSP1E3D1 nanodiscs showing a relative population of slow lipids in the nanodiscs.

Table 1
Thermodynamic parameters and lipid population distributions calculated for POPC and DMPC nanodiscs (both MSP1D1 and MSP1E3D1). Relative population of the label present in the surroundings of fast lipids (at 310 K), the standard Gibbs energy ΔG (at 310 K), enthalpy ΔH, and entropy ΔS changes connected to the transfer of the spin label from a fast to a slow population of lipids.

Nanodiscs	N_{fast}	$\Delta G^0_{Fast\rightarrow Slow}$	$\Delta H^0_{Fast\rightarrow Slow}$	$\Delta S^0_{Fast\rightarrow Slow}$
	[%]	[kcal mol^{-1}]	[kcal mol^{-1}]	[kcal mol^{-1}]
POPC MSP1D1	66.3	0.42	4.41	−15.5
DMPC MSP1D1	54.4	0.50	4.95	−17.5
POPC MSP1E3D1	69.4	0.11	5.82	−19.1
DMPC MSP1E3D1	55.6	0.14	5.69	−18.8
Liposomes			$\Delta H^0_{Gel\rightarrow Liquid}$ [kcal mol^{-1}]	
DMPC			6.0 ± 2.4	
POPC			5.8 ± 1,0	

the number of lipids in the direct neighborhood of the MSP (see SI), showing that around 30% of lipids are in direct contact with the MSP (Fig. S22, Table S5). This estimate agrees with the experimentally estimated number of DMPC molecules in direct contact with the MSPs. Here it was assumed that the number of lipids in contact with the MSP is approximately the same as the number of lipids in the liquid-disordered state below the main phase transition temperature: for DMPC-based nanodiscs, there are about 34% lipids in contact with the MSP, in both MSP1D1 and MSP1E3D1 nanodiscs (Fig. S10).

4. Conclusions

The results of our studies reveal the structure of nanodiscs to be more complicated than previously anticipated. While the global increase in the ordering of lipid acyl chains in nanodiscs is comparable to the effect of cholesterol on lipid bilayers, which has been shown previously [29,30,33,53], the current study provides a more resolved picture separating the structural and dynamical parameters as well as connecting the lateral and transversal inhomogeneity of lipid bilayers in nanodiscs. This was possible due to the combination of EPR spectroscopy with atomistic molecular dynamics simulations.

The results of MD simulations and EPR measurements revealed that there are three distinct populations of lipids in nanodiscs. The first population is comprised of disordered lipids in direct contact with the MSP (lipids in the nanodisc boundary). These lipids are evident in EPR data, where they remain in the fluid state even at temperatures below T_m. The lipid bilayer is thinnest in this part of the nanodisc.

Next, at temperatures above T_m, two distinct populations of fast and slow lipids are observed in experimental data. MD simulations indicate that the population of fast lipids is a group of peripheral lipids located in a 3 nm thick belt neighboring the MSP. In this region, the lipid acyl chain order gradually increases when one moves from the MSP towards the center of the nanodisc. This group comprises about 60% (Table S5) of lipids in the nanodiscs.

Finally, the central portion of the nanodiscs is characterized by significant order, comprising the remaining fraction of lipids. This region is evident in EPR measurements as slow lipids due to the order of the central region that slows down dynamic motions. Importantly, central lipids in nanodiscs are also more ordered than lipids in liposomes or planar bilayers, and the level of order is comparable to the

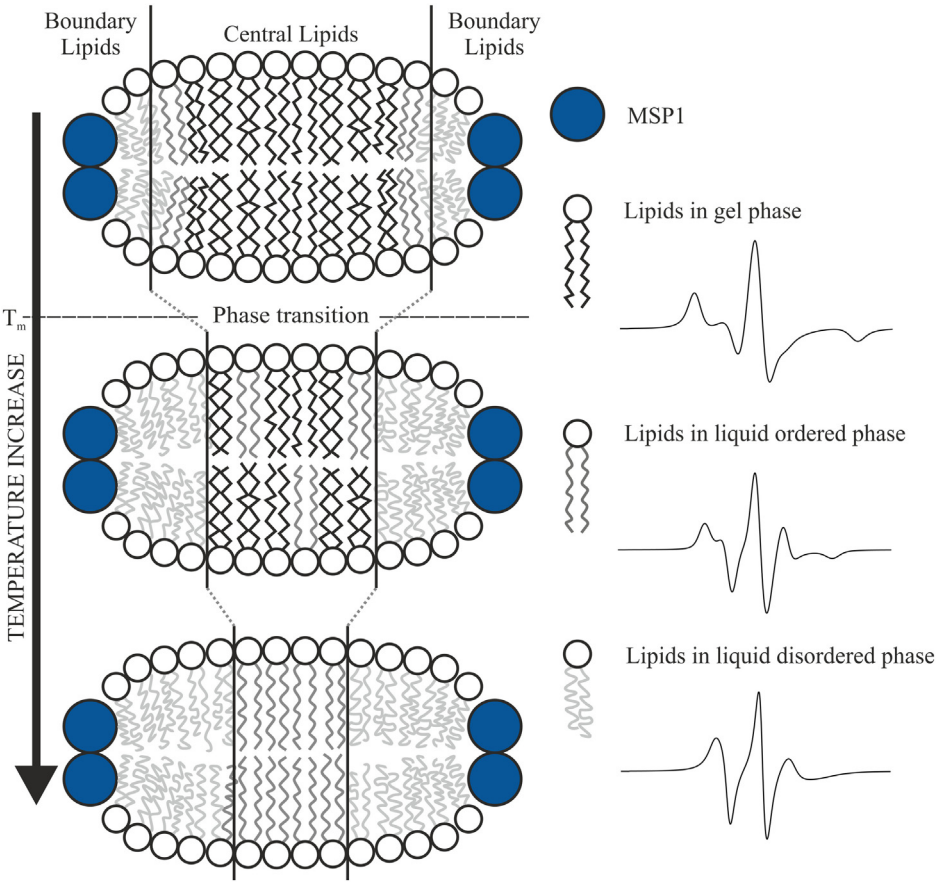

Fig. 7. Schematic representation of lateral ordering of lipids in nanodiscs in different temperature regimes (the arrow denotes increasing temperature; the main phase is transition marked with a dashed line) (left panel). In nanodiscs below T_m, a spectral component characteristic to both the liquid-ordered and the gel state can be observed. At higher temperatures (POPC at 310 K, DMPC around 303–313 K), gel components change to match values corresponding to the liquid-disordered phase. Spectral components corresponding to different phases are shown on the right.

liquid-ordered phase in cholesterol-rich lipid membranes. Not surprisingly, the enthalpies of transitions between fast and slow lipids are comparable to the enthalpies related to the main phase transition.

The inhomogeneity in lipid order and thickness across the nanodiscs affects their hydration. The central lipids are more hydrophobic due to higher ordering and denser packing of the lipids, whereas the boundary lipids, which form the curved part of the bilayer in a nanodisc, are more hydrated.

Given that nanodiscs have become an indispensable tool in membrane protein research, the knowledge of their structure is crucial for understanding its influence on target membrane proteins. This has also been demonstrated in recent and ongoing structural studies of nanodiscs [53,65]. Further, the hydration of lipid headgroups [28], thickness of the bilayer [60,61] and packing of acyl chains [60,66] modulate the activity of membrane proteins.

The observations of the present study provide novel insights into the spatial heterogeneous structure of nanodiscs, which can be utilized in several different ways. For instance, the size of nanodiscs can be used to control the degree of lipid packing, while maintaining an optimal lipid composition for a target protein. A reconstituted membrane protein could replace the lipids in the central region of a nanodisc, which depending on the size of a nanodisc would be characterized by a different packing state. This can be used as a way of mimicking membranes with different protein concentrations. Second, nanodiscs modulate the structure of lipid headgroups in the proximity of membrane proteins, which allows one to study the role of the membrane in mediating the interactions of small, amphipathic ligands with membrane proteins. Finally, both packing and hydration can be further controlled through temperature, which, as shown in the present work, influences the lipid distribution between differently structured lipid populations.

Declaration of competing interest

The authors declare that they have no known competing financial interests or personal relationships that could have appeared to influence the work reported in this paper.

Acknowledgements

For computational resources, we wish to thank the CSC–IT Center for Science Ltd. (Espoo, Finland). We also would like to thank Z. Pakosz for the help with the preparation of the EPR related figures and the final scheme. This work was funded by the Academy of Finland (Center of Excellence in Biomembrane Research (grant no. 307415)) (T.R., I.V.), European Research Council (Advanced Grant project CROWDED-PROLIPIDS (grant no. 290974)) (I.V.), the Helsinki Institute of Life Science Fellow project (I.V.), and Sigrid Juselius Foundation (I.V.). P.S., A.P. and A.W.B. acknowledge the Faculty of Biochemistry, Biophysics and Biotechnology of Jagiellonian University, a partner of the Leading National Research Center (KNOW) supported by the Ministry of Science and Higher Education.

Appendix A. Supplementary data

Supporting Information contains experimental details, additional data including additional information on spectral fitting and MD runs, as well as Figs. S1–S24, and Tables S1–S5. Supplementary data to this article can be found online at https://doi.org/10.1016/j.bbamem.2020.183420.

References

[1] I.G. Denisov, S.G. Sligar, Nanodiscs in membrane biochemistry and biophysics,

Chem. Rev. 117 (2017) 4669–4713.
[2] R. Kuai, L.J. Ochyl, K.S. Bahjat, A. Schwendeman, J.J. Moon, Designer vaccine nanodiscs for personalized cancer immunotherapy, Nat. Mater. 16 (2016) 489–496.
[3] M. Numata, Y.V. Grinkova, J.R. Mitchell, H.W. Chu, S.G. Sligar, D.R. Voelker, Nanodiscs as a therapeutic delivery agent: inhibition of respiratory syncytial virus infection in the lung, Int. J. Nanomedicine 8 (2013) 1417–1427.
[4] Y.S. Grewal, M.J.A. Shiddiky, S.M. Mahler, G.A. Cangelosi, M. Trau, Nanoyeast and other cell envelope compositions for protein studies and biosensor applications, ACS Appl. Mater. Interfaces 8 (2016) 30649–30664.
[5] P. Wang, A.Y. Chang, V. Novosad, V.V. Chupin, R.D. Schaller, E.A. Rozhkova, Cell-free synthetic biology chassis for nanocatalytic photon-to-hydrogen conversion, ACS Nano 11 (2017) 6739–6745.
[6] R. Fernandez-Leiro, S.H.W. Scheres, Unravelling biological macromolecules with cryo-electron microscopy, Nature 537 (2016) 339–346.
[7] I.G. Denisov, S.G. Sligar, Nanodiscs for structural and functional studies of membrane proteins, Nat. Struct. Mol. Biol. 23 (2016) 481–486.
[8] Z. Cournia, T.W. Allen, I. Andricioaei, B. Antonny, D. Baum, G. Brannigan, N.V. Buchete, J.T. Deckman, L. Delemotte, C. del Val, R. Friedman, P. Gkeka, H.C. Hege, J. Hénin, M.A. Kasimova, A. Kolocouris, M.L. Klein, S. Khalid, M.J. Lemieux, N. Lindow, et al., Membrane protein structure, function, and dynamics: a perspective from experiments and theory, J. Membr. Biol. 248 (2015) 611–640.
[9] L. Fagerberg, K. Jonasson, G. Von Heijne, M. Uhlén, L. Berglund, Prediction of the human membrane proteome, Proteomics 10 (2010) 1141–1149.
[10] O. Vit, J. Petrak, Integral membrane proteins in proteomics how to break open the black box? J. Proteome 153 (2017) 8–20.
[11] C.S. Tautermann, GPCR structures in drug design, emerging opportunities with new structures, Bioorg. Med. Chem. Lett. 24 (2014) 4073–4079.
[12] R. Lappano, M. Maggiolini, G protein-coupled receptors: novel targets for drug discovery in cancer, Nat. Rev. Drug Discov. 10 (2011) 47–60.
[13] H. Yin, A.D. Flynn, Drugging membrane protein interactions, Annu. Rev. Biomed. Eng. 18 (2016) 51–76.
[14] A. Stetsenko, A. Guskov, An overview of the top ten detergents used for membrane protein crystallization, Crystals 7 (2017) 197.
[15] M. Caffrey, A comprehensive review of the lipid cubic phase or in meso method for crystallizing membrane and soluble proteins and complexes, Acta Crystallogr. Sect. F Struct. Biol. Commun. 71 (2015) 3–18.
[16] P.J. Loll, Membrane proteins, detergents and crystals: what is the state of the art? Acta Crystallogr. Sect. F Struct. Biol. Commun. 70 (2014) 1576–1583.
[17] S.C. Lee, S. Khalid, N.L. Pollock, T.J. Knowles, K. Edler, A.J. Rothnie, O. R.T.Thomas, T.R. Dafforn, Encapsulated membrane proteins: a simplified system for molecular simulation, Biochim. Biophys. Acta Biomembr. 1858 (2016) 2549–2557.
[18] P. Jin, D. Bulkley, Y. Guo, W. Zhang, Z. Guo, W. Huynh, S. Wu, S. Meltzer, T. Cheng, L.Y. Jan, Y.N. Jan, Y. Cheng, Electron cryo-microscopy structure of the mechanotransduction channel NOMPC, Nature 547 (2017) 118–122.
[19] R. Wild, J. Kowal, J. Eyring, E.M. Ngwa, M. Aebi, K.P. Locher, Structure of the yeast oligosaccharyltransferase complex gives insight into eukaryotic N-glycosylation, Science 359 (2018) 545–550.
[20] T. Gutmann, K.H. Kim, M. Grzybek, T. Walz, Ü. Coskun, Visualization of ligand-induced transmembrane signaling in the full-length human insulin receptor, J. Cell Biol. 217 (2018) 1643–1649.
[21] G. Enkavi, M. Javanainen, W. Kulig, T. Róg, I. Vattulainen, Multiscale simulations of biological membranes: the challenge to understand biological phenomena in a living substance, Chem. Rev. 119 (2019) 5607–5774.
[22] B. Augustyn, P. Stepien, C. Poojari, E. Mobarak, A. Polit, A. Wisniewska-Becker, T. Róg, Cholesteryl hemisuccinate is not a good replacement for cholesterol in lipid nanodiscs, J. Phys. Chem. B 123 (2019) 9839–9845.
[23] M.L. Nasr, D. Baptista, M. Strauss, Z.Y.J. Sun, S. Grigoriu, S. Huser, A. Plückthun, F. Hagn, T. Walz, J.M. Hogle, G. Wagner, Covalently circularized nanodiscs for studying membrane proteins and viral entry, Nat. Methods 14 (2016) 49–52.
[24] I.G. Denisov, Y.V. Grinkova, A.A. Lazarides, S.G. Sligar, Directed self-assembly of monodisperse phospholipid bilayer nanodiscs with controlled size, J. Am. Chem. Soc. 126 (2004) 3477–3487.
[25] B.A. Chromy, E. Arroyo, C.D. Blanchette, G. Bench, H. Benner, J.A. Cappuccio, M.A. Coleman, P.T. Henderson, A.K. Hinz, E.A. Kuhn, J.B. Pesavento, B.W. Segelke, T.A. Sulchek, T. Tarasow, V.L. Walsworth, P.D. Hoeprich, Different apolipoproteins impact nanolipoprotein particle formation, J. Am. Chem. Soc. 129 (2007) 14348–14354.
[26] T.K. Ritchie, Y.V. Grinkova, T.H. Bayburt, I.G. Denisov, J.K. Zolnerciks, W.M. Atkins, S.G. Sligar, Chapter 11 reconstitution of membrane proteins in phospholipid bilayer nanodiscs, Methods Enzymol. 464 (2009) 211–231.
[27] M. Manna, M. Niemelä, J. Tynkkynen, M. Javanainen, W. Kulig, D.J. Müller, T. Róg, I. Vattulainen, Mechanism of allosteric regulation of β_2-adrenergic receptor by cholesterol, Elife 5 (2016) 1–21.
[28] R. Dawaliby, C. Trubbia, C. Delporte, M. Masureel, P. Van Antwerpen, B.K. Kobilka, C. Govaerts, Allosteric regulation of G protein-coupled receptor activity by phospholipids, Nat. Chem. Biol. 12 (2016) 35–39.
[29] K. Mörs, C. Roos, F. Scholz, J. Wachtveitl, V. Dötsch, F. Bernhard, C. Glaubitz, Modified lipid and protein dynamics in nanodiscs, Biochim. Biophys. Acta Biomembr. 1828 (2013) 1222–1229.
[30] Y. Wada, N. Matsuzaki, H. Endo, T. Handa, Static and dynamic properties of phospholipid bilayer nanodiscs, J. Am. Chem. Soc. 131 (2009) 8308–8312.
[31] O.H.S. Ollila, M. Louhivuori, S.J. Marrink, I. Vattulainen, Protein shape change has a major effect on the gating energy of a mechanosensitive channel, Biophys. J. 100 (2011) 1651–1659.
[32] I.G. Denisov, B.J. Baas, Y.V. Grinkova, S.G. Sligar, Cooperativity in cytochrome P450 3A4: linkages in substrate binding, spin state, uncoupling, and product formation, J. Biol. Chem. 282 (2007) 7066–7076.
[33] P. Stepien, A. Polit, A. Wisniewska-Becker, Comparative EPR studies on lipid bilayer properties in nanodiscs and liposomes, Biochim. Biophys. Acta Biomembr. 1848 ((2015) 60–66.
[34] M. Raguz, L. Mainali, W.J. O'Brien, W.K. Subczynski, Lipid-protein interactions in plasma membranes of fiber cells isolated from the human eye lens, Exp. Eye Res. 120 (2014) 138–151.
[35] W.K. Subczynski, A. Wisniewska, W.K. Subczynski, A. Wisniewska, J.J. Yin, J.S. Hyde, A. Kusumi, Hydrophobic barriers of lipid bilayer membranes formed by reduction of water penetration by alkyl chain unsaturation and cholesterol, Biochemistry 33 (1994) 7670–7681.
[36] S. Jo, T. Kim, V. Iyer, W. Im, CHARMM GUI: a web based graphical user interface for CHARMM, J. Comput. Chem. 29 (2008) 1859–1865.
[37] J. Lee, X. Cheng, J.M. Swails, M.S. Yeom, P.K. Eastman, J.A. Lemkul, S. Wei, J. Buckner, J.C. Jeong, Y. Qi, S. Jo, V.S. Pande, D.A. Case, C.L. Brooks, A.D. MacKerell, J.B. Klauda, W. Im, CHARMM-GUI input generator for NAMD, GROMACS, AMBER, OpenMM, and CHARMM/OpenMM simulations using the CHARMM36 additive force field, J. Chem. Theory Comput. 12 (2016) 405–413.
[38] A.D. MacKerell, D. Bashford, M. Bellott, R.L. Dunbrack, J.D. Evanseck, M.J. Field, S. Fischer, J. Gao, H. Guo, S. Ha, D. Joseph-McCarthy, L. Kuchnir, K. Kuczera, F.T.K. Lau, C. Mattos, S. Michnick, T. Ngo, D.T. Nguyen, B. Prodhom, W.E. Reiher, et al., All-atom empirical potential for molecular modeling and dynamics studies of proteins, J. Phys. Chem. B 102 (1998) 3586–3616.
[39] M. Pourmousa, R.W. Pastor, Molecular dynamics simulations of lipid nanodiscs, Biochim. Biophys. Acta Biomembr. 1860 (2018) 2094–2107.
[40] R.M. Islam, M. Pourmousa, D. Sviridov, S.M. Gordon, B. Edward, L.A. Freeman, B.S.P. Jr, R.W. Pastor, A.T. Remaley, Structural properties of apolipoprotein A-I mimetic peptides that promote ABCA1- dependent cholesterol efflux, Sci. Rep. 8 (2018) 2956.
[41] M. Pourmousa, H.D. Song, Y. He, J.W. Heinecke, J.P. Segrest, R.W. Pastor, Tertiary structure of apolipoprotein A-I in nascent high-density lipoproteins, Proc. Natl. Acad. Sci. U. S. A. 115 (2018) 5163–5168.
[42] A. Debnath, L.V. Schäfer, Structure and dynamics of phospholipid nanodiscs from all-atom and coarse-grained simulations, J. Phys. Chem. B 119 (2015) 6991–7002.
[43] H.J.C. Berendsen, J.P.M. Postma, W.F. van Gunsteren, A. DiNola, J.R. Haak, Molecular dynamics with coupling to an external bath, J. Chem. Phys. 81 (1984) 3684–3690.
[44] S. Nosé, A unified formulation of the constant temperature molecular dynamics methods, J. Chem. Phys. 81 (1984) 511–519.
[45] W.G. Hoover, Canonical dynamics: equilibrium phase-space distributions, Phys. Rev. A 31 (1985) 1695–1697.
[46] M. Parrinello, A. Rahman, Polymorphic transitions in single-crystals - a new molecular-dynamics method, J. Appl. Phys. 52 (1981) 7182–7190.
[47] T. Darden, D. York, L. Pedersen, Particle mesh Ewald: an $N \cdot \log(N)$ method for Ewald sums in large systems, J. Chem. Phys. 98 (1993) 10089–10092.
[48] B. Hess, H. Bekker, H.J.C. Berendsen, J.G.E.M. Fraaije, LINCS: a linear constraint solver for molecular simulations, J. Comput. Chem. 18 (1997) 1463–1472.
[49] J.B. Klauda, R.M. Venable, J.A. Freites, J.W. O'Connor, D.J. Tobias, C. Mondragon-Ramirez, I. Vorobyov, A.D. MacKerell, R.W. Pastor, Update of the CHARMM all-atom additive force field for lipids: validation on six lipid types, J. Phys. Chem. B 114 (2010) 7830–7843.
[50] M.J. Abraham, T. Murtola, R. Schulz, S. Páll, J.C. Smith, B. Hess, E. Lindahl, Gromacs: high performance molecular simulations through multi-level parallelism from laptops to supercomputers, SoftwareX 1–2 (2015) 19–25.
[51] W. Humphrey, A. Dalke, K. Schulten, VMD-visual molecular dynamics, J. Mol. Graph. 14 (1996) 33–38.
[52] N. Castillo, L. Monticelli, J. Barnoud, D.P. Tieleman, Free energy of WALP23 dimer association in DMPC, DPPC, and DOPC bilayers, Chem. Phys. Lipids 169 (2013) 95–105.
[53] D. Martinez, M. Decossas, J. Kowal, L. Frey, H. Stahlberg, E.J. Dufourc, R. Riek, B. Habenstein, S. Bibow, A. Loquet, Lipid internal dynamics probed in nanodiscs, ChemPhysChem 18 (2017) 2651–2657.
[54] L.M. Stimson, L. Dong, M. Karttunen, A. Wisniewska, M. Dutka, T. Róg, Stearic acid spin labels in lipid bilayers: insight through atomistic simulations, J. Phys. Chem. B 111 (2007) 12447–12453.
[55] I.G. Denisov, M.A. McLean, A.W. Shaw, Y.V. Grinkova, S.G. Sligar, Thermotropic phase transition in soluble nanoscale lipid bilayers, J. Phys. Chem. B 109 (2005) 15580–15588.
[56] I. Siuda, D.P. Tieleman, Molecular models of nanodiscs, J. Chem. Theory Comput. 11 (2015) 4923–4932.
[57] A.W. Shaw, M.A. McLean, S.G. Sligar, Phospholipid phase transitions in homogeneous nanometer scale bilayer discs, FEBS Lett. 556 (2004) 260–264.
[58] M. Stepniewski, A. Bunker, M. Pasenkiewicz-Gierula, M. Karttunen, T. Róg, Effects of the lipid bilayer phase state on the water membrane interface, J. Phys. Chem. B 114 (2010) 11784–11792.
[59] J. Tuchtenhagen, W. Ziegler, A. Blume, Acyl chain conformational ordering in liquid-crystalline bilayers: comparative FT-IR and 2H-NMR studies of phospholipids differing in headgroup structure and chain length, Eur. Biophys. J. 23 (1994) 323–335.
[60] J.D. Pilot, J.M. East, A.G. Lee, Effects of bilayer thickness on the activity of diacylglycerol kinase of Escherichia coli, Biochemistry 40 (2001) 8188–8195.
[61] F. Cornelius, Modulation of Na,K-ATPase and Na-ATPase activity by phospholipids and cholesterol I steady-state kinetics, Biochemistry 40 (2001) 8842–8851.
[62] S. Kapoor, A. Werkmüller, C. Denter, Y. Zhai, J. Markgraf, K. Weise, N. Opitz,

R. Winter, Temperature-pressure phase diagram of a heterogeneous anionic model biomembrane system: results from a combined calorimetry, spectroscopy and microscopy study, Biochim. Biophys. Acta Biomembr. 1808 (2011) 1187–1195.
[63] L. Mainali, J.B. Feix, J.S. Hyde, W.K. Subczynski, Membrane fluidity profiles as deduced by saturation-recovery EPR measurements of spin-lattice relaxation times of spin labels, J. Magn. Reson. 212 (2011) 418–425.
[64] Z. Huang, F.C. Szoka, Sterol-modified phospholipids: cholesterol and phospholipid chimeras with improved biomembrane properties, J. Am. Chem. Soc. 130 (2008) 15702–15712.
[65] S. Bibow, Y. Polyhach, C. Eichmann, C.N. Chi, J. Kowal, S. Albiez, R.A. McLeod, H. Stahlberg, G. Jeschke, P. Güntert, R. Riek, Solution structure of discoidal high-density lipoprotein particles with a shortened apolipoprotein A-I, Nat. Struct. Mol. Biol. 24 (2017) 187–193.
[66] A.P. Starling, J.M. East, A.G. Lee, Effects of phosphatidylcholine fatty acyl chain length on calcium binding and other functions of the (Ca2+ − Mg2+)-ATPase, Biochemistry 32 (1993) 1593–1600.